STUDY OF THE TRANSIENT TEMPERATURE PROFILES INDUCED BY CHANGES OF THE WELDING PARAMETERS DURING ALUMINUM TWO PLATE ARC BUTT-WELDING

Yetzirah Urthaler

Pedro Viggiani

Carolina Payares

Luis Rojas-Solórzano*

Universidad Simón Bolívar
Departamento de Mecánica
(*) Departamento de Conversión de Energía
Apdo. 89000, Caracas, 1080-A, Venezuela
Tlf: 58-2-906-4023, Fax: 58-2-906-4062
e-mail: urthaler@usb.ve

ABSTRACT

The numerical study and calculation of transient temperatures developing during the arc-welding process of 6063 T5 aluminum plates is presented. The mathematical model is based on the differential energy conservation equation. The governing equation is solved via numerical simulation using the finite control volume method to obtain the three dimensional and transient temperature profiles induced during the welding process. The moving heat source is considered as represented by a centered Gaussian-Bell distribution, while the base material is assumed to be homogeneous and isotropic with temperature-dependent thermal properties. Radiation and convection are computed and introduced into the model through the boundary conditions as an empirical temperature-dependent correlation. Phase-change phenomenon is included as a discontinuity in the material specific heat. Computed results show the influence of the variation of the welding parameters such as the arc power and welding speed on the computed transient temperatures, penetration and process efficiency.

NOMENCLATURE

C_p	specific heat;
d	weld bead depth (mm);
E	arc-weld voltage (Volt);
e	metal sheet thickness;
$GMAW$	gas metal arc welding;
h_{eff}	effective heat transfer coefficient;
I	arc-weld electric current (A);
K	thermal conductivity;
p	penetration (mm);
p_{num}, p_{exp}	penetration values obtained by simulation and experimental procedures, respectively (mm);
q_o	electrode power (Watts);
Q_o	effective heat per unit of time out of the electrode (Watts);
r_b	arc-weld effective radius;
t	time (seg);
T	temperature (^{o}K);
T_s	surface temperature (^{o}K);
T_{inf}	surrounding temperature (^{o}K);
T_{sol}	minimum temperature at which liquid phase appears (^{o}K);
T_{liq}	minimum temperature at which there is only liquid phase (^{o}K);
V	electrode translation speed (m/seg);
w	weld bead width (mm);
xyz	spatial coordinates referred to a fixed-to-plate reference system;
z_o, z_f	initial and final position of the source, respectively;
$xy\xi$	spatial coordinates referred to a fixed-to-electrode reference system;
ε	material emissivity;
δ	delta Dirac's function;
η	electrode overall efficiency;
τ	factor to calculate the position of the heat source at t= 0;
ρ	material density;

INTRODUCTION

A wide variety of weld-joints made of 6063 T5 aluminum is found in numerous engineering applications such as cryogenics, unfired pressure vessels, marine components, pipes and irrigation pipes. When such structures are fabricated by welding process, very deep temperature gradients arise in the vicinity of the weld. This differential heating, followed by cooling to ambient temperature causes residual stresses that remain in the structure after it has returned to ambient temperature. In addition to residual stresses, the welding process causes distortion, that is, geometrical imperfections which tend to reduce the material strength. Thermal gradients also determine the geometry of the weld bead, the penetration, the size of grains, segregation, intergranular cracking and porosity of the fusion and heat affected zone, which are used to estimate the strength and the fracture behavior of the weld-joints. In order to predict the mechanical properties of the weld joints, the residual stresses and distortions produced in a plate by welding, it is necessary first to predict the transient temperature profiles that develop in the plate in order to perform the stress analysis.

The present work focuses on the calculation of the transient temperatures developing during the arc-welding process of 6063 T5 aluminum plates. The temperature distribution is numerically determined by solving the heat flow equilibrium equation. Very large temperature variations take place during the welding process causing the physical properties of the plate material to change with temperature. Thus, the problem is highly nonlinear and its analytical solution is difficult to obtain. The governing equation is solved numerically using the finite control volume method to obtain the three dimensional and transient temperature profiles induced during the welding process. The moving heat source is considered as represented by a centered Gaussian-Bell distribution, while the base material is assumed to be homogeneous and isotropic with temperature-dependent thermal properties. Radiation and convection are computed and introduced into the model through the boundary conditions as an empirical temperature-dependent correlation. Phase-change phenomenon is included as a discontinuity in the material specific heat. In particular, this paper is concerned with the study of the effect of the variation of the welding parameters on the computed temperature, penetration and efficiency. The welding variables taken into account are the source power and welding speed.

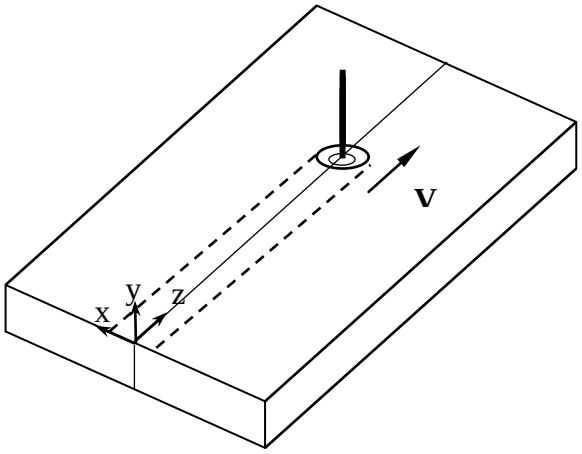

Fig. 1. Simplified scheme of welding process

BACKGROUND

In the study of the arc-length welding process, temperature profiles are of primary relevance since, for a given material and joint design, the temperature distribution determines the size of the melted region, the heat affected area, the resultant microstructure and associated mechanical properties, the residual stresses and the plastic deformation of the base plate.

Various numerical techniques based on the finite difference method have been used to calculate the temperature distribution in steel welded thin plates (Krutz and Zegerlin 1978; Kou 1981; Oreper and Szekely 1984; Tsao and Wu 1988; Ramanan and Korpela 1990; Ule *et al.* 1990; Ravichandran *et al.* 1996). Besides, the finite element method has also been employed to solve the problem (Friedman 1975; Mani and Shukla 1981; Zacharia *et al.* 1989; Chidiac *et al*. 1944; Goldak *et al.* 1986). Payares *et al*. (2000) performed the simulation of the heat transfer phenomena by means of a finite control volume technique. However, remarkably few results for the thermal simulation of aluminum butt joints have been published (Payares *et al* 2000; Hval, 1998).

Experimental results about the influence of the welding variables on the weld bead geometry and penetration have been obtained for steels, e.g., McGlone and Chaqwick (1978); Shmoda (1978); Chandel and Bala (1986) and Chandel (1987). A very limited amount of research related to the weld joint penetration behavior using the GMAW (gas metal arc welding) process for aluminum weld-joints has been reported in previous literature (Burch 1958; Datsko 1977; Yasuda 1991; Malyn 1995; Kiyohara 1997 and Payares *et al*. 1999).

The aim of this work is to provide a deeper understanding of the effects of changes of the welding parameters on the heat transfer phenomena that take place during aluminum arc butt-welding, based on a shorter time-scale, more versatile and a less expensive procedure than found by experimental means. It is expected that this analysis will later help to the development of numerical correlations among the welding variables enabling the derivation of convenient welding procedures and resulting in the prediction of the mechanical properties and fracture behavior of the weld joints.

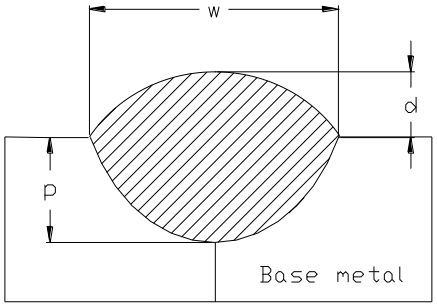

Fig. 2. Scheme of a weld bead geometry and penetration in a butt joint.

MATHEMATICAL MODEL

Figure 1 shows the schematics of the plate-to-plate butt-welding process using arc welding. The heat source (plasm arc) moves along the upper surface above the two plates interface, at a constant velocity *V*.

The two-plate butt-welding problem is modeled as a heat source translating at a constant speed along the z-axis. The governing equation is the energy equation, given in Cartesian coordinates as

$$\frac{\partial}{\partial x}\left(K\frac{\partial T}{\partial x}\right)+\frac{\partial}{\partial y}\left(K\frac{\partial T}{\partial y}\right)+\frac{\partial}{\partial z}\left(K\frac{\partial T}{\partial z}\right)+Q=\rho C_p\frac{\partial T}{\partial t} \quad (1)$$

The material thermal properties (i.e., K and C_p) are considered as temperature dependent, homogeneous and isotropic. Figure 3, shows K and C_p values used in the simulations (Lho *et al.* 1991). The analysis neglects the internal heat dissipation due to eddy currents associated to the arc-weld magnetic field.

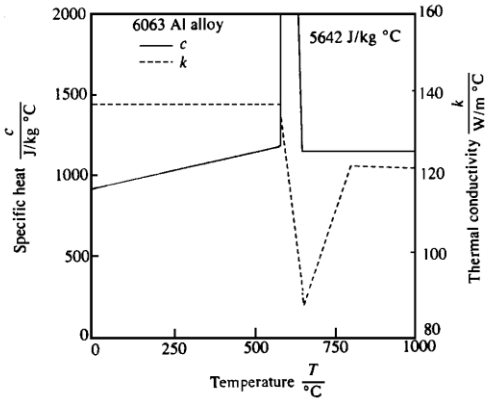

Fig. 3. Thermal conductivity and specific heat as a function of temperature for aluminum alloy Al 6063.

Boundary conditions

Symmetry along the z-axis leads to

$$\frac{\partial T}{\partial x}=0\text{, at } x=0 \quad (2)$$

The Gauss-bell-like heat source over upper surface (Fig. 4), is given by Eq. (3) as follows

$$q(x,\xi)=\frac{3Q_o}{\pi r_b^2}\exp(-3(x^2+\xi^2)/r_b^2) \quad (3)$$

where,

$$\xi=z-V(\tau+t) \quad (4)$$

$$q_o=E\,I \quad (5)$$

$$Q_o=\eta q_o \quad (6)$$

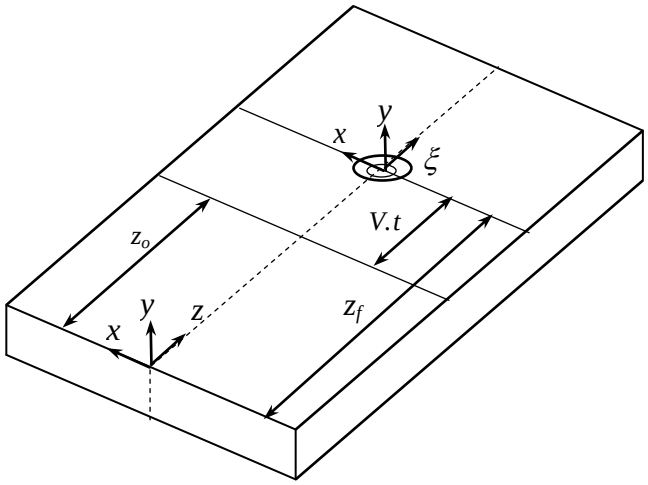

Figure 4. Computational reference coordinate system

Sometimes, for the sake of clarity, it is convenient to express the heat source equation in *xyz* coordinates. Thus, Eq. (3) becomes

For $x^2+\xi^2\le r_b^2$,

$$q(x,z,t)=\frac{3Q_o}{\pi r_b^2}\exp(-3(x^2+(z-V(\tau+t))^2)/r_b^2) \quad (7)$$

And, for $x^2+\xi^2>r_b^2$,

$$q(x,z,t)=0 \quad (8)$$

On the upper side of the plate, outside the circle of radius r_b, and within the rest of the surfaces, but the lower side, there is heat flux leaving the metal sheet due to convection and radiation, given by:

$$q_{eff}=-h_{eff}(T_s-T_{\inf}) \quad (9)$$

where the effective heat transfer coefficient can be computed as (Na and Lee, 1987),

$$h_{eff}=-0.00241\varepsilon T_s^{1.61} \quad (10)$$

On the lower side, the temperature gradient in the *y*-direction is zero:

$$\frac{\partial T}{\partial y} = 0 \text{ for } y = -e \qquad (11)$$

Latent (Fusion) heat

Latent heat, ΔH_f, is modeled as a singularity in the metal specific heat equation (Pardo and Weckman, 1989)

$$C_p = C_p(T) + \Delta H_f \, \delta(T - T_{liq}) \qquad (12)$$

Table 4. Constants used in simulations

T_{liq}	925 [K]
T_{sol}	855 [K]
T_{inf}	295 [K]
Density ρ	2700 [kg/m^3]
Emissivity ε	0.9

Numerical Simulation

The transient energy equation was solved using a finite-volume-based code (CFX4.2^{TM}). The optimal time-step was set up to obtain an acceptable convergence at an affordable computational time capturing the small time-scales of the problem. The computation of gross or integral quantities (i.e., weld penetration and width) and the introduction of temperature-dependent physical properties (i.e., $K(T)$ and $C_p(T)$), required the creation and validation of Fortran subroutines (CFX4.2^{TM} Solver Manual, 1997). Constant values used to run the simulations (i.e., T_{liq}, T_{sol}, T_{inf}, density and emissivity) are shown in Table 4. The mesh independence of computational results was verified and afterwards, the final computational domain consisted of 240.000 regular control volumes. A pentium III, 450 MHz-192 MB ram PC ran every simulation in 60 min., average. The process efficiency (η), was adjusted to obtain the best fit in weld penetration between the numerical model and experiments (Payares, 1985) previously run using Aluminum 6063 test probes of 6.35 mm thick, 50.8 mm wide and 80 mm long. Three sets of parameters involving the maximum and minimum values of the variation ranges for the welding variables were considered in that study (see table 5). More details on the experiments and the efficiency fitting procedure might be found in Payares (1985) and Payares *et al*. (1999), respectively.

Table 5. Penetration and efficiency numerical results for the selected study cases. Comparison with experimental penetration results.

V[cm/min]	E[V]	I[A]	q_o[W]	η	p_{num} [mm]	p_{exp}[mm]
50	24	210	5040	0,92	4,55	4,51
50	18	150	2700	0,50	1,16	1,08
95	24	210	5040	0,40	2,01	1,97

NUMERICAL RESULTS

The numerical results depicted in the following figures aim to the analysis of the influence of the welding parameters (i.e. welding speed, electrode power) on the transient temperatures developing during the welding process. This influence is also investigated on the penetration and on the process efficiency.

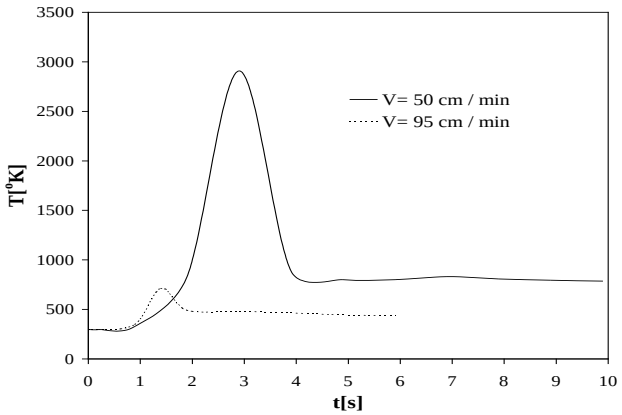

Fig. 5. Temperature vs. time at z=20mm for different V values (y=0,E=24 Volt, I=210A)

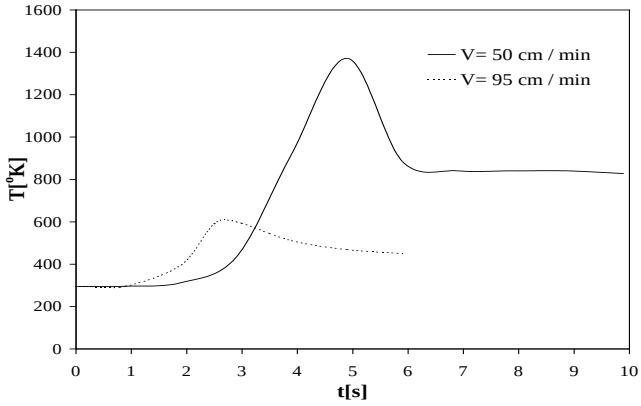

Fig. 6. Temperature vs. time at z=40mm for different V values (y=0, E=24 Volt, I=210A)

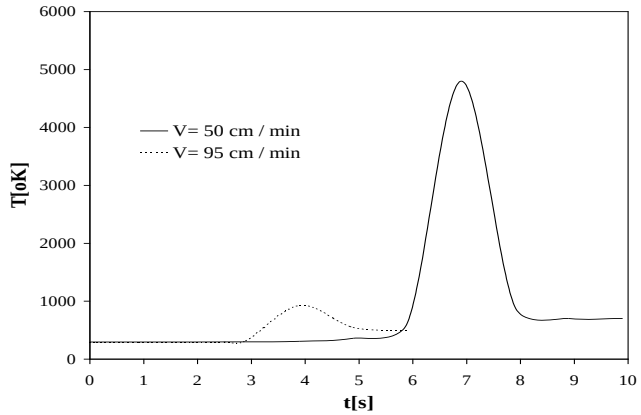

Fig. 7. Temperature vs. time z=60mm for different V values (y=0, E=24 Volt, I=210A)

Figs. 5, 6 and 7 show the influence of the welding speed on the temperature-time plots at a constant $\mathbf{q_o}$ value, for three points located on the top plane along the z-axis (z=20mm, z=40 mm, z=60mm). Temperature peaks, which correspond to the maximum temperatures, take place when the electrode is positioned above the considered point. The main time-scale corresponds to the period of time required by the electrode to move along the total length of the plate.

As the welding speed increases the effective heat input per unit of time decreases. Therefore, the maximum temperatures decrease significantly. It should be quoted that for higher values of welding speed, maximum temperatures are reached in a smaller period of time. Thus, the curves shown in those figures are shifted.

Temperature peaks are smaller for points located in regions away from the edges. These results suggest that, the process of heat transfer through the plate considerably outweighs that of heat transfer from the plate by convection and radiation. Thus, close to the edges, heat transfer by conduction becomes less significant, causing an increment in the maximum temperatures. Temperature peaks are steeper for regions near the ending welding edge due to the preheating effect, in comparison with computed temperatures for regions in the vicinity of the beginning welding edge.

Figs. 8 and 9 show the temperature distribution on the top and longitudinal planes, for two electrode positions at a constant welding speed. Since the problem is geometrically symmetrical, only half of the plate is shown.

Fig. 8. Temperature [°K] distribution on the longitudinal symmetry plane and top plane at t=0.3 sec (V= 50 cm/min, E=24 Volt, I=210 A)

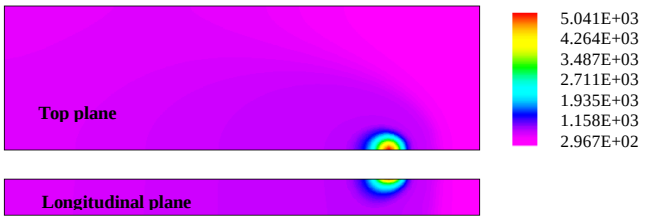

Fig. 9. Temperature [°K] distribution on the longitudinal symmetry plane and top plane at t=7.2 sec (V= 50 cm/min, E=24 Volt, I=210 A)

Examination of these figures confirms that the preheated area increases as the electrode moves toward the ending edge. Consequently, an increase in the maximum temperature is presented.

Comparison between figures 10 and 11 demonstrates that for higher welding speeds, the heat affected zone decreases due to the reduction of heat transferred from the heat source into the plate.

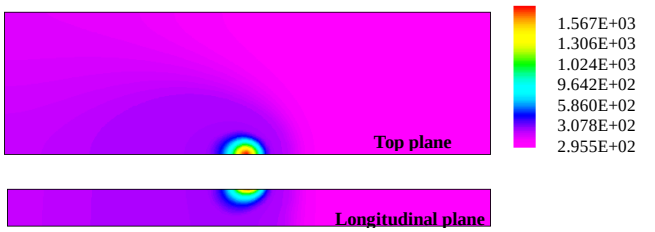

Fig. 10. Temperature[°K] distribution on the longitudinal symmetry plane and top plane at t=4.8 sec (V= 50 cm/min, E=24 Volt, I=210 A)

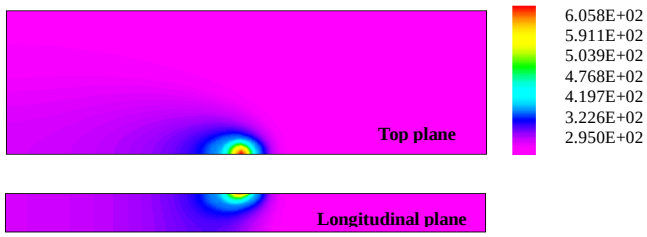

Fig. 11. Temperature[°K] distribution on the longitudinal symmetry plane and top plane at t=2.5 sec (V= 95 cm/min, E=24 Volt, I=210 A)

Similar temperature-time curves (figs. 12 to 14) were obtained varying the electrode power $\mathbf{q_o}$, while the welding speed was kept constant. As the electrode power increases, the effective heat into the plate increases. Thus, for example, Fig. 12 shows how an 87% increase in the electrode power, causes the temperature to triple at z=20mm on the top surface.

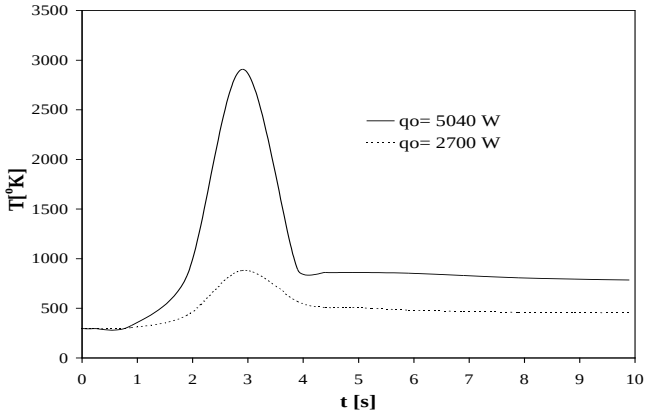

Fig. 12. Temperature vs. time at z=20mm for different q_o values (y=0,V= 50 cm / min)

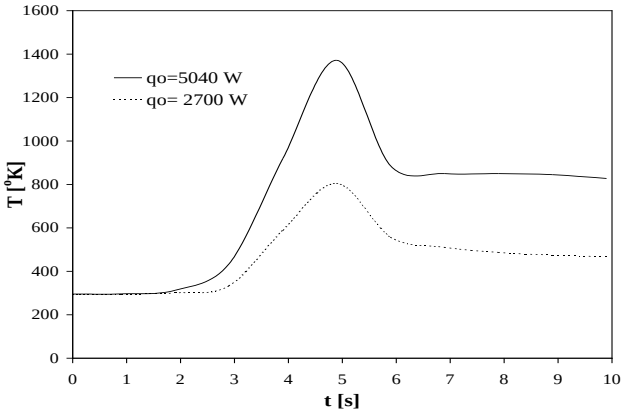

Fig. 13. Temperature vs. time at z=40mm for different q_o values (y=0, V= 50 cm / min)

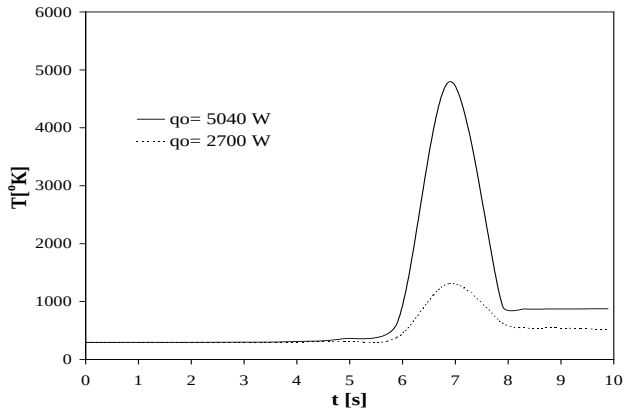

Fig. 14. Temperature vs. time at z=60mm for different q_o values (y=0,V= 50 cm / min)

Temperature increments due to the increase of the electrode power or due to the decrease in welding speed derive into an augmentation of the fusion zone and penetration, as shown in Figs. 15 and 16.

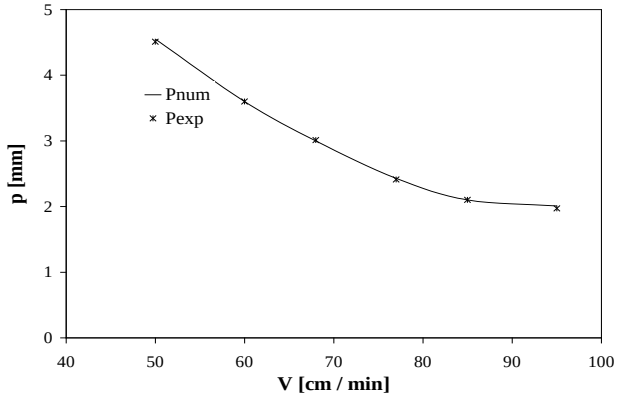

Fig. 15. Penetration vs. welding speed (E=24 Volt, I=210)

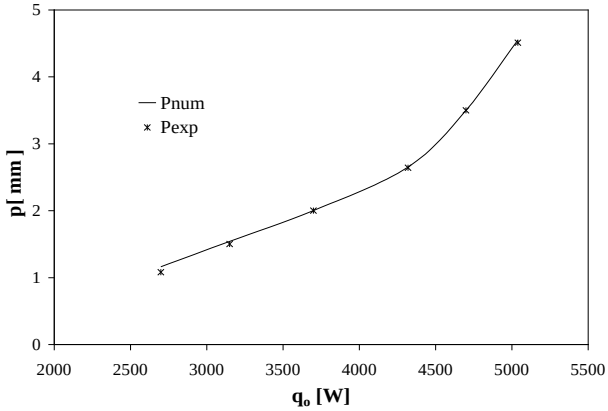

Fig. 16. Variation of the penetration with the electrode power (V= 50 cm / min)

The heat source welding efficiency, defined as the ratio between the effective heat flux into the plate and the gross heat dissipated by the source, increases as the effective heat entering the plate increases. This effect takes place as the welding speed decreases or as the electrode power increases (Figs. 17 and 18).

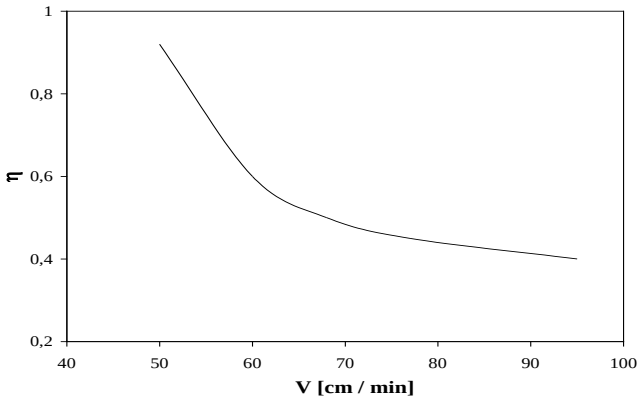

Fig. 17. Heat source efficiency vs. welding speed (E=24 Volt, I=210)

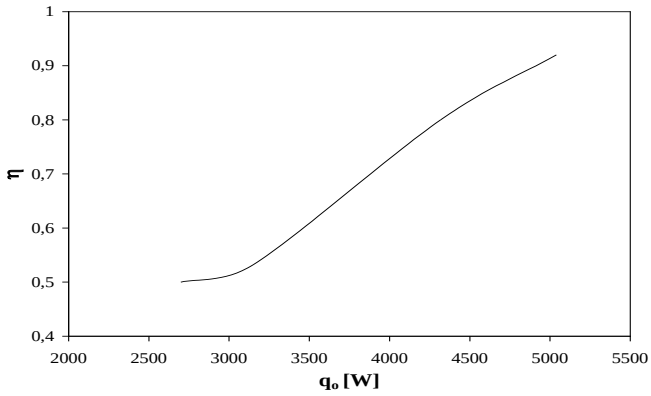

Fig. 18. Heat source efficiency vs. electrode power (V= 50 cm / min)

CONCLUSIONS

The numerical study and calculation of transient temperatures developing during the arc butt-welding process of 6063 T5 aluminum plates has been presented. The physical problem was modeled and the resulting governing differential equation and appropriate boundary conditions were solved using a finite volume numerical solver. The heat source efficiency is obtained by fitting numerical results to experiments obtained in a previous work.

Computational results show the influence of welding variables on the computed temperature distribution. Thus, it is found that for a constant electrode power (constant heat source supply), an increment in the welding speed decreases the maximum temperature that arises over the plate surface and within, during the welding process. In contrast, for a constant welding speed, an increment in the electrode power originates an increment in the maximum temperature.

Maximum temperatures are registered in regions located near the ending welding edge where preheating and free air convection effects are combined. The surface temperature as a function of time, at a particular location, reaches a peak value when the electrode is positioned above the considered location, indicating the fast response or high conductivity of the plate.

It was found that the increment in the welding speed or the decay in the electrode power supply causes a reduction both in the penetration and heat source efficiency, and vice-versa.

The preliminary results shown in this report aim to build a more robust and realistic mathematical model to simulate the highly complex two-plate arc butt-welding process. Thus, further investigation is currently ongoing on that direction.

ACKNOWLEDGEMENT

This research was carried out with the computational resources provided by the Center for Fluid Mechanics and Applications at the Universidad Simón Bolívar (CEMFA-USB), Caracas-Venezuela. The authors also wish to thank Dr. Miguel Reyes for his comments to this work.

REFERENCES

AEA Technology, 1997, CFX 4.2 Solver Manual.

Burch, W.L., 1958, "The effect of weld speed on strength of aluminum joints", *AWS Annual Spring Meeting* , St. Louis, Apr. 14-18, pp..361s-367s.

Chandel R.S., 1987, "Prediction of weld metal dilution from SAW parameters", *Welding Review*, Vol. 6., No.1, pp. 45-46.

Chandel, R.S. and Bala, S.R., 1986, "The relationships between SAW parameters and weld bead size", *Physical Metallurgy Research Laboratory Report*, PMRL 86-38 (J), CANMET, EMR, Ottawa, Canada.

Datsko J., 1977, *Materials in Design and Manufacturing*, Malloy Inc. Ann Arbor, Michigan, pp. 8-1 to 8-9.

Goldak, J., Chakravarti, A.and Bibby, M., 1984, " A new finite element model for welding heat sources, *Metallurgical Transactions B*, Vol. 15,pp. 299-305.

Hval, M., Thaulow, J.H., Lange, S.H., Hoydal, H. and Zhang, Z.L., 1998, " Numerical modeling of ductile fracture behavior in aluminum weldments", Welding Journal, Vol. 77, pp208s-216s.

Kiyohara, T., Okada, T., Wakino, Y., and Yamamoto, H., 1977, "On the satabilization of GMA welding of aluminum", *Welding Journal*, Vol. 56, No.1, pp. 21-28.

Lho, T. J. and Na, S. J., 1991, "A study on three-dimensional transient heat flow in circumferential GTA welding of pipes using periodicity conditions", *Journal of Engineering of Manufacture*, Vol. 205, pp. 271-278.

Malyn, V., 1995, " Study of metallurgical phenomena in the HAZ of 6061 T6 aluminum welded joints", *Welding Research Supplements*, Vol. 74, No.9, pp. 305s-318s.

Mc Glone, J.C., and Chaqwick D.B., 1978, "The submerged arc butt welding of mild steel", Part 2: " The prediction of weld bead geometry from the procedure parameters*", The Welding Institute Report*, 80/1978/PE.

Na, S. J. and Lee, S. Y., 1987, "A study on three-dimensional analysis of the transient temperature distribution in gas tungsten arc", *Journal of Engineering of Manufacture*, Vol. 201, pp. 149-156.

Pardo E. and Weckman, D.C., 1989, "Prediction of weld pool and reinforcement dimensions of GMA welds using a finite the analysis of marine pipelines during laying operations", *Metallurgical Transactions B J. of Pipelines*, Vol. 20, pp. 937-947.

Payares, C., *Modelo para la determinación de la penetración e influencia de los parámetros de operación en la geometría del cordón en soldaduras a tope de Aluminio 6063 T5*, Internal Report (in Spanish), Universidad Simón Bolívar, Caracas-Venezuela.

Payares, M.C., De Barros, C. and Muñoz-Escalona, P., 1998, "Mathematical model for the prediction of the penetration in butt joints for aluminum 6063 T5", *Fatigue, Environmental Factors and New Materials*, PVP Vol. 374, pp 23-27.

Payares, M.C., Dorta, M. and Muñoz-Escalona, P., 1999, " Influence of the welding variables on the mechanical properties in butt joints for aluminum", *Fracture, Fatigue and Weld Residual Stresses*, PVP Vol. 393, pp. 339-344.

Payares, M.C., Rojas-Solórzano, L. and Viggiani, P., 2000, " Numerical simulation of the heat penetration in two plate arc welding", *Métodos Numéricos en Ingeniería y Ciencias Aplicadas*, pp. 61-68.

Shmoda, T., and Doherty J., 1978, " The relationship between arc welding parameters and weld bead geometry – a literature survey", *The Welding Institute Report*, 74/1978/PE.

Yasuda, K., 1991, " Welding conditions of aluminum welding", *J. Light Met. Constr*., Vol. 29, No.10, pp. 8-12.